AIAA JOURNAL
Vol. 37, No. 5, May 1999

Direct Numerical Simulation of Unsteady Finite-Span Hydrofoil Flow

Chao-Tsung Hsiao* and Laura L. Pauley†
Pennsylvania State University, University Park, Pennsylvania 16802-1412

The tip-vortex flow over a finite-span hydrofoil with laminar separation on the hydrofoil surface was numerically studied by computing the three-dimensional unsteady Navier–Stokes equations. The computations were direct numerical simulations of all resolvable structures without adding a turbulence model. The topological structure of unsteady separated flow and the influence of the unsteady laminar separated flow on the tip vortex for both swept and unswept hydrofoils were qualitatively investigated. The secondary flow induced by the swept planform played an important role in the unsteadiness of the tip vortex. The interaction between the tip vortex and the unsteady laminar separated flow became stronger as the sweep angle was increased.

Nomenclature

Ar	= aspect ratio (based on semispan)
c	= chord length
N	= number of nodal points
N'	= number of half-node points
Re	= chord Reynolds number
S	= number of saddle points
S'	= number of half-saddle points
t	= nondimensional time
x, y, z	= Cartesian coordinate system
α	= angle of attack
ξ, η, ζ	= generalized coordinate system

I. Introduction

THE tip-vortex flowfield in the vicinity of the tip region is a very complicated three-dimensional viscous flow phenomenon. The details of the flow in the tip region are important in determining the performance of the lifting surfaces in both aerodynamic and hydrodynamic applications. To date, the understanding of the tip-vortex formation, however, is primarily limited to time-averaged results. Although the unsteadiness of the tip vortex has recently been studied experimentally,[1,2] insufficient data collection and incomplete measurement of the pressure field usually led the investigation to be inconclusive.

According to the previous study of Arndt et al.,[3] one mechanism producing unsteadiness of the tip vortex is hypothesized to be the laminar boundary-layer separation on the finite-span hydrofoil surface. From observation of a singing vortex on a fully cavitating vortex core, Maines and Arndt[2] suggested that the spanwise shedding vortices from the laminar separation bubble interacted with the tip vortex and caused low-frequency pressure fluctuations in the tip-vortex core. In a numerical study, therefore, accurate resolution of the laminar separated flow on the hydrofoil surface is necessary to predict accurately the unsteady pressure field in the tip-vortex core.

Lin and Pauley[4] used unsteady Navier–Stokes computations to study the laminar separation bubble on a two-dimensional airfoil at low Reynolds numbers ($Re < 2 \times 10^5$). The computations were direct numerical simulations of all resolvable structures without the addition of a turbulence model. The favorable comparison between their numerical results and experimental data suggested that the unsteady large-scale structure, in the form of vortex shedding, controls the laminar separation and the small-scale turbulence plays only a secondary role. Wilson and Pauley[5] used a large-eddy simulation (LES) to study the influence of small-scale turbulence on the structure of the separation bubble. They found that the addition of the LES model did not significantly alter the separation bubble structure at low Reynolds numbers. This result suggests that the direct numerical simulation can offer a good qualitative understanding of the unsteady features of the tip vortex at low Reynolds numbers by resolving only the large-scale motions of the separated flow.

The secondary flow crossing the tip of a finite-span hydrofoil always causes the laminar separation along the span to become highly three-dimensional near the tip. The analysis of three-dimensional unsteady separation is itself a challenging task. In the two-dimensional case separation leads to flow reversal and recirculation, which is often viewed as a vortex with its axis parallel to that of the body. Under certain conditions the vortex detaches periodically to give rise to the phenomenon of vortex shedding. In the three-dimensional case the separated shear layer may also roll up to form a streamwise vortex, but neither the point of origin of the vortex nor the location of its axis can be readily determined in some cases because the vorticity varies smoothly throughout the flowfield and there are no discontinuities that define the extent of the vortices and their core. Although the use of topological rules and bifurcation theory[6,7] have provided a mathematical framework for studying separated flows, most studies are dedicated to steady flows and simple geometries. The topological structures of unsteady separation and vortex shedding are not well established and understood. Recent unsteady three-dimensional separation studies are described in Refs. 8–10.

The first task of the present study is to describe the topological structure of unsteady laminar separation on the hydrofoil surface from numerical results. The interaction between the unsteady laminar separation and the tip vortex is described in the subsequent section. Two hydrofoil planforms are considered in the present study. A swept hydrofoil is used to study the unsteadiness of the laminar separation and the tip vortex. An unswept (rectangular) hydrofoil is considered to study the effect of hydrofoil planform on the unsteadiness.

II. Geometry and Numerical Aspects

Two different hydrofoil planforms, rectangular and swept hydrofoil (30-deg sweep angle), are considered in the present study to investigate how laminar separation on the hydrofoil surface modifies the tip-vortex flow. Both hydrofoils have an Eppler 387 cross section with a round tip and an aspect ratio (based on semispan) $Ar = 1.5$ without twist or taper.

A three-dimensional unsteady incompressible Navier–Stokes flow solver INS3D-UP, developed by Rogers et al.,[11] is applied without turbulence modeling to simulate numerically the laminar spanwise separation and the tip-vortex flow. INS3D-UP is a finite

Received May 27, 1997; revision received Dec. 1, 1998; accepted for publication Jan. 2, 1999.

*Research Assistant; currently Research Scientist, Dynaflow, Inc., 7210 Pindell School Road, Fulton, MD 20759.

†Associate Professor, Department of Mechanical Engineering. Senior Member AIAA.

difference code based on the artificial-compressibility method. In the artificial-compressibility method a time derivative of pressure is added to the continuity equation to couple it with the momentum equations. As a consequence, a hyperbolic system of equations is formed and can be solved using a time-marching scheme. The spatial differencing of the convective terms uses a fifth-order accurate flux-difference splitting based on Roe's method.[12] A second-order central differencing is used for the viscous terms. The resulting system of algebraic equations is solved by a Gauss–Seidel line-relaxation method in which several line-relaxation sweeps through the computational domain are performed before the solution is updated at the new pseudo time step. This method can be marched in pseudo time to reach a steady-state solution when a divergence-free velocity field is obtained. To obtain a time-dependent solution, a subiterative procedure for pseudo time needs to be performed at each physical time step. In INS3D-UP a first-order Euler implicit method is used for the pseudo time while a second-order Euler implicit method is used for the physical time. In the present study the time-accurate solution was acquired when the maximum velocity divergence was less than 1.0×10^{-3}.

Because the present study considers both the tip-vortex flow and the laminar separation flow on the hydrofoil surface, a sufficiently dense grid must exist around the tip vortex and on the hydrofoil surface. To obtain an appropriate grid distribution, an H-H grid topology with two blocks (one for the pressure side and one for the suction side) and a combination of algebraic and elliptic grid generation techniques developed by Hsiao and Pauley[13] are applied to create the grid.

Performing numerical experiments to obtain grid-independent and time-accurate solutions in the three-dimensional unsteady flow is nearly impossible, as pointed out by Mehta.[14] Furthermore, the lack of experimental data on the three-dimensional unsteady finite-span hydrofoil flow also prohibits the validation of numerical solution. Some numerical parameters are therefore estimated from the three-dimensional steady computations and two-dimensional unsteady computations. In the present study the grid within the tip vortex and laminar separation bubble needs to be carefully considered. Dacles-Mariani et al.[15] carried out a full Navier–Stokes simulation of a laminar vortex and showed that an average of 15–20 grid points across the vortex core was required to resolve the tip vortex adequately. For the unsteady laminar separation flow Lin[16] has conducted extensive computations on a two-dimensional foil at low Reynolds number ($Re < 2 \times 10^5$). Lin found that, to obtain a grid-independent and time-accurate solution, a grid with at least 40 grid points in both the normal and streamwise directions within the primary separation bubble and a time-step size corresponding to 150 intervals within one shedding cycle need to be used. This number of grid points and time-step size, however, will make unsteady three-dimensional calculation unpractical. To relax the burden of memory and CPU time, a reduced grid with 25 grid points in the normal direction and 21 grid points in the streamwise direction within the primary separation bubble was used. A time-step size corresponding to 23 intervals ($\Delta t = 1.0 \times 10^{-2}$ where t is nondimensionalized by inflow velocity and chord length) within one shedding cycle was applied in the present computations.

To justify the grid number and time-step size used in the present study, a grid and time-step size independence study was conducted for a two-dimensional case. A two-dimensional test case that doubled the grid points in the streamwise and normal directions modified the velocity field by less than 2% at any specified phase in the shedding cycle. The shedding cycle frequency decreased by 2% when the coarse grid was used. Decreasing the time step from 1.0×10^{-2} to 1.5×1.0^{-3} reduced the shedding frequency by 3%. The modification of the velocity field at any specified phase in the shedding frequency was also less than 3%. Comparison of the coarse-grid velocity field with Lin's results at the same phase in the shedding cycle gave a maximum error of less than 5%. The prediction of the vortex shedding frequency, however, differed by 13%. The cause of this discrepancy could not be identified. We hypothesized that a prediction of the laminar shear-layer instability leading to vortex shedding is particularly sensitive to the numerical method and the domain used. Lin conducted a two-dimensional computation, whereas the present study approximated a two-dimensional flow by using only three grid points in the spanwise direction and applying a periodic boundary condition. Because the present study of the three-dimensional unsteady flow offers a better qualitative understanding of the tip-vortex unsteadiness, some numerical error will be tolerated. For the three-dimensional computation 85 grid points including 55 points on the hydrofoil surface are distributed in the spanwise direction. The complete three-dimensional grid has $155 \times 85 \times 61$ on the suction side and $155 \times 85 \times 41$ on the pressure side, which yields a total of 1,343,850 grid points in the computational domain that has the inlet, outlet, and farfield boundaries at five chord lengths away from the foil. The three-dimensional view of the grid distribution is shown in Fig. 1. Streamwise-grid clustering can be seen at the leading and trailing edge of the hydrofoil. Grid clustering in the spanwise direction is applied at the hydrofoil tip.

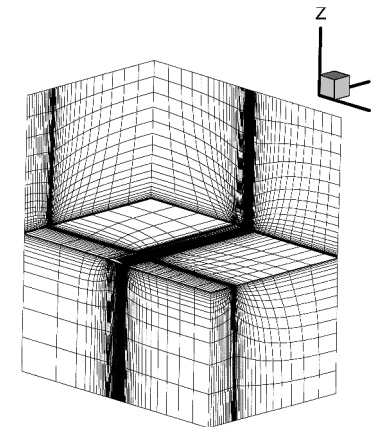

Fig. 1 Three-dimensional view of the grid distribution (plotted in every other grid point).

The present study considers a three-dimensional impulsively started flow. An uniform flow, therefore, is applied as the initial condition. For the boundary conditions, freestream velocity and pressure are specified at the far-field boundary and the inflow boundary, whereas first-order extrapolation of all variables is used at the outflow boundary. At the root section a symmetry boundary condition is applied. On the solid hydrofoil surface no-slip flow and zero normal pressure gradient conditions are used. All computations are conducted at $Re = 1.0 \times 10^5$ and $\alpha = 4$ deg. As the computation proceeds, the tip vortex and laminar separation on the hydrofoil surface start to develop.

III. Three-Dimensional Unsteady Separated Flow

There is a difficulty in conceptually visualizing three-dimensional steady and unsteady flow patterns. A description of flow patterns using singular or critical point concepts[6,17] provides a framework and methodology for overcoming this difficulty. Critical points are classified into two types: nodal N and saddle points S. Nodal points may be further subdivided into two subclasses: nodes and foci. If critical points occur on the boundary, then they are defined as half-nodes N' and half-saddles S'. The ideas of critical-point theory are applicable to the limiting streamlines or skin-friction lines on a body and to the flow above the body surface. Tobak and Peake[6] summarized five topological rules for a body that is simply connected and immersed in an uniform flow. The present study applies the following two rules to describe the topological structure of the three-dimensional unsteady separated flow. First, the skin-friction lines on an isolated closed three-dimensional body must satisfy

$$\Sigma N - \Sigma S = 2 \tag{1}$$

Second, streamlines on a two-dimensional plane cutting a three-dimensional body must satisfy

$$\left(\Sigma N + \tfrac{1}{2}\Sigma N'\right) - \left(\Sigma S + \tfrac{1}{2}\Sigma S'\right) = -1 \tag{2}$$

These topological rules are defined originally for steady flow. However, Hui and Tobak[8] showed that the topological properties of the unsteady flow separation at any instant time are also governed by the same rules that govern separation in the steady flow. The

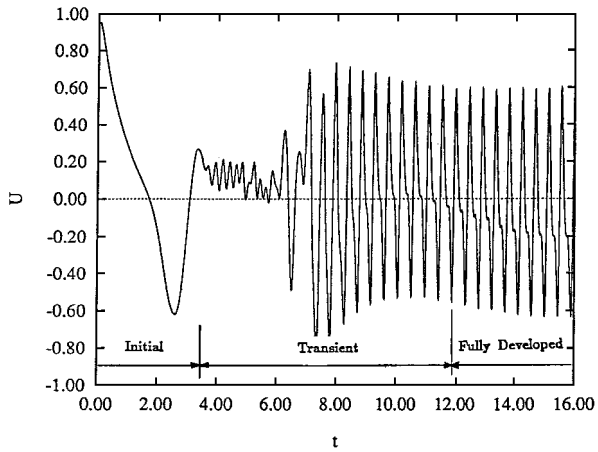

Fig. 2 Three stages of the velocity history during the development of the unsteady separated flow on a two-dimensional foil.

correctness of a topological sketch, therefore, can always be checked by noting whether the results conform with the known constraints given by the critical-point theory.

According to the numerical study of the two-dimensional unsteady separated flow on a foil at low Reynolds number $Re = 1.0 \times 10^5$, the development of unsteady separation can be divided into three stages: initial, transient, and fully developed. Figure 2 shows the velocity history monitored at a location downstream of the separation bubble and indicates the stages of separation development. When the computation is started from freestream conditions without any perturbation, a separation bubble will begin to develop on the foil surface at the initial stage. As the computation continues, a vortex will begin to shed from the separation bubble because of the instability of the free shear layer. As the vortex passes the monitoring point, the velocity at the monitoring point begins to oscillate in time. After a transient period the oscillation will reach a periodic limit cycle at the fully developed stage.

A. Development of Limiting Streamline on Surface

For the three-dimensional flow the development of unsteady separation can be studied using the topological history of limiting streamlines on the hydrofoil surface. Pauley[10] showed that the limiting streamlines at the wall also satisfied the topological rule during the unsteady separation development.

The development of the limiting streamlines at the initial and the early transient stages for the swept hydrofoil is shown in Figs. 3a and 3b. The calculated limiting-streamline results are accompanied by sketches that interpret their topological structure. During the initial development, the topological structure of the limiting streamlines is simple. Additional nodes and saddles, corresponding to vortex shedding, start to form at the transient stage.

Figure 3a shows that at the initial stage $t = 2.8$ the three-dimensional separation bubble already occurs across the span. There are two convergent lines along the span: One is near the midcord, and the other one is near the trailing edge. The terms *first and second convergent lines* will refer to the leading and trailing separation lines hereafter. A complex flow structure is found near the tip region because the swept hydrofoil induces a secondary flow from the root to the tip while the pressure difference between the pressure and suction sides drives a secondary flow over the tip and forms the tip vortex. The topological structure of the separation is illustrated by a sketch showing the characteristic lines and nodal and saddle points. To describe the complete topological structure, one can imagine this finite-span hydrofoil as half of a full-span hydrofoil that is symmetric along the center line, i.e., the root of the finite-span hydrofoil. The sum of nodal points from the full-span hydrofoil, therefore, always exceeds that of saddle points by two. This indicates that the topological structure satisfies Eq. (1).

At the early transient stage $t = 3.4$ as shown in Fig. 3b, additional separation and reattachment lines start to form between the leading and trailing separation lines beyond the midspan. As time progresses, additional separation and reattachment lines form and increase in length. These additional separation lines are formed by spanwise vortices shedding from the leading separation bubble. The spanwise vortices travel downstream and interact with the trailing separation bubble. In addition to the spanwise vortex, the focus of the leading separation has degenerated to a node and begins shedding during the transient stage. By $t = 11.4$ the spanwise vortex shedding from the leading separation bubble becomes more regular, and the extent of the spanwise vortex along the span becomes constant, i.e., the spanwise vortex does not extend further toward the root.

B. Vortex Shedding and Pairing

Investigating the flow structure at the fully developed stage is of most interest because it describes typical operating conditions. As seen experimentally by Henk et al.[18] and computationally by Pauley et al.,[19] the flow structure of the initial and transient stages may depend on the start-up conditions, whereas the fully developed flow does not. In the two-dimensional pressure-induced separation studies of Pauley et al.,[19] a slow exponentially applied adverse-pressure gradient produced the same ultimate separation structure as an impulsively applied gradient but with time lag. In the two-dimensional case the fully developed stage is defined when the velocity history monitored within the boundary layer behind the separation bubble reaches a limit cycle. To examine the development of separation on the three-dimensional hydrofoil, streamwise velocity histories were recorded at several locations as shown in Fig. 4. The velocity histories at locations 1 and 3 reach repeatable limit cycles while those at locations 2 and 4 remained in random oscillations. Because the computation was terminated at $t = 12.5$, we are still not certain whether a repeatable limit cycle can be reached at locations 2 and 4. Further discussion of this region will be included later.

To determine the vortex shedding frequency, three additional locations (A, B, C), as shown in Fig. 4, are used to record velocity histories directly behind the separation bubble where no vortex pairing occurs. The velocity histories at these three locations are shown in Fig. 5. Figure 5 shows that the vortex shedding frequency varies slightly across the span.

In Fig. 4 each spanwise convergent line represents the leading edge of a spanwise vortex. By following a traveling convergent line, one can find that the convergent line will break into segments, reconnect with other segments, and/or merge into another convergent line. Three possible processes are illustrated in Fig. 6. From the two-dimensional study of Lin,[16] the velocity of the traveling vortex is influenced by the streamwise adverse-pressure gradient. The streamwise adverse-pressure gradient tends to decelerate the velocity of the traveling vortex. Because the magnitude of the streamwise adverse-pressure gradient varies across the span, one expects that the spanwise vortex will travel at different velocities across the span, and this will cause the spanwise vortex line to stretch along the span. To see the vortex pairing, one can consider two neighboring spanwise vortices (leading and trailing vortices) traveling downstream. Because the leading vortex will be decelerated by a stronger streamwise adverse-pressure gradient, the trailing vortex may reach the leading vortex, and the two vortices merge. During the period when the trailing vortex stretches and merges with its leading vortex, the convergent lines follow one of the three processes shown in Fig. 6.

To illustrate the vortex pairing, the limiting streamlines on the x–z plane cutting the hydrofoil at $\eta = 20$ (as indicated in Fig. 4) for five different time steps are shown in Fig. 7. Figure 4 shows that the separation structure is nearly two-dimensional and more organized between the leading separation line and about 0.75 chord length downstream of the leading edge. The flow-structure development can, therefore, be easily demonstrated by using the topological structure of vortex shedding and pairing obtained from the two-dimensional case. In the two-dimensional case the phenomenon of vortex shedding includes the growth of the primary vortex, development of the counter-rotating vortex, pinching of the primary vortex, and subsequent vortex transport. The process of vortex pairing occurs when the trailing vortex catches up to the leading vortex, rolls over it, and finally merges. Although vortex shedding and pairing are caused by different flow mechanisms, they produce the same development of the flow topology except in reverse. Figure 8 shows

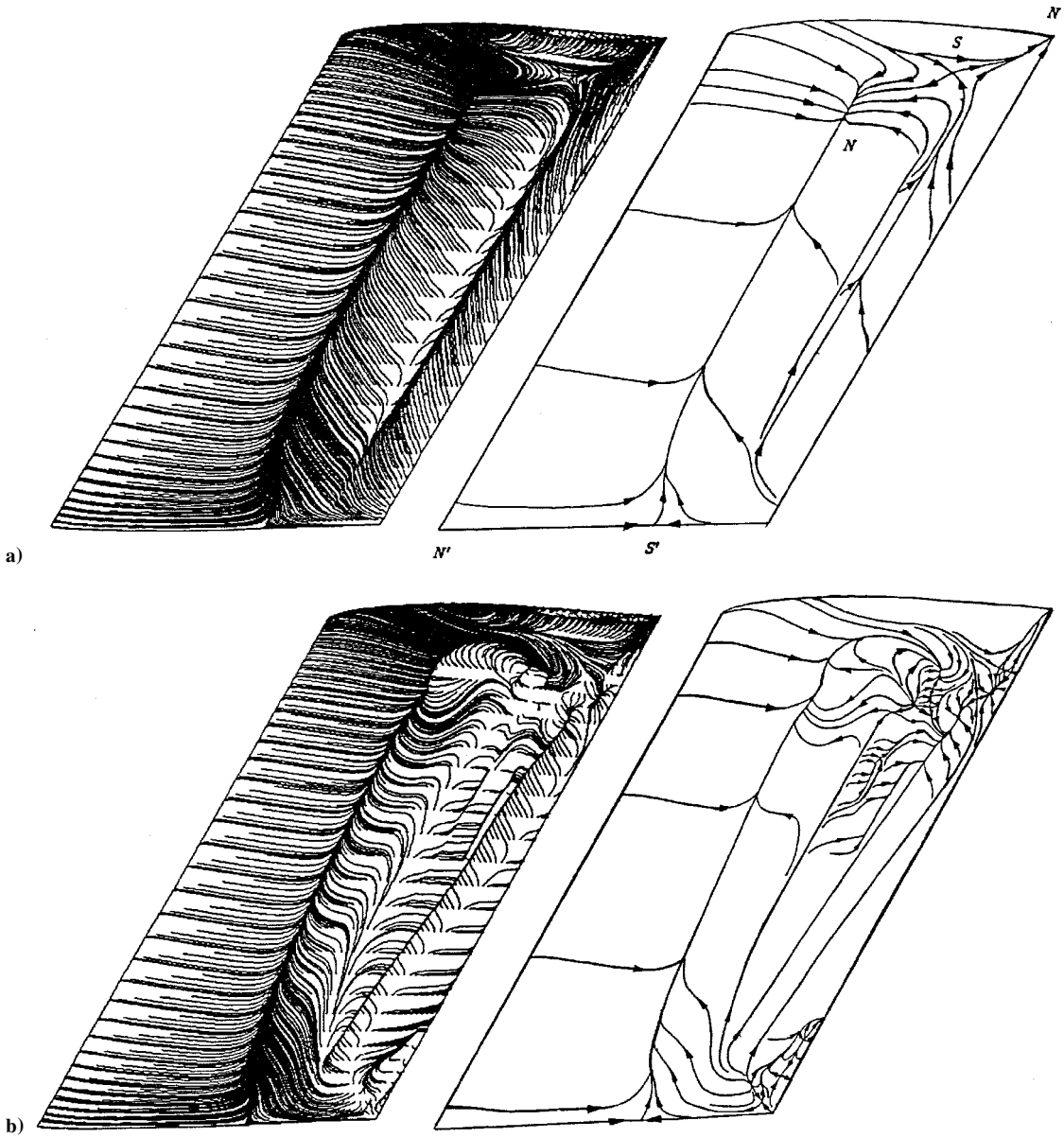

Fig. 3 Development of the limiting streamlines and the sketch of the topological structure for the swept hydrofoil at a) the initial stage $t = 2.8$ and b) the early transient stage $t = 3.4$.

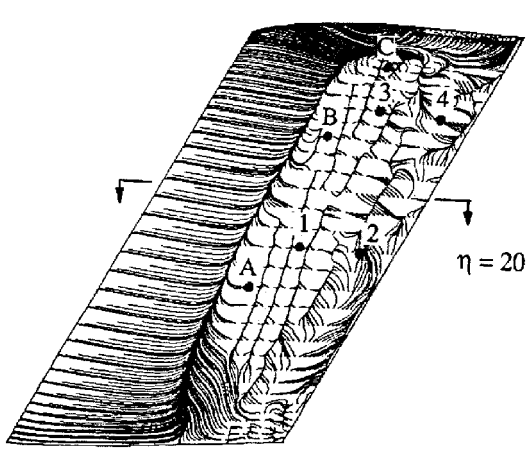

Fig. 4 Surface limiting streamlines at $t = 11.56$ and locations used to monitor the velocity history.

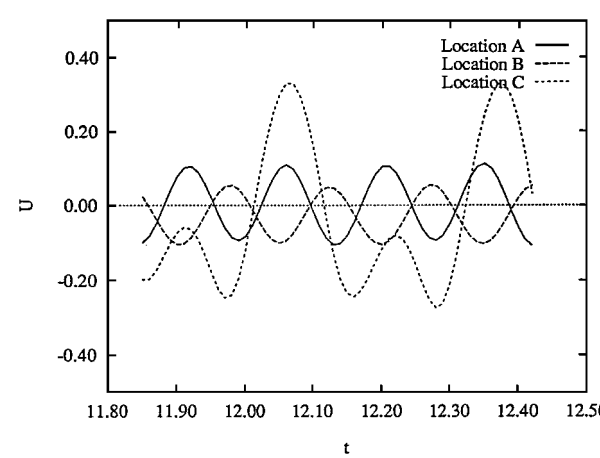

Fig. 5 Expanded views of the limit-cycle oscillations monitored at 3×10^{-3} chord lengths above the hydrofoil surface for three different locations.

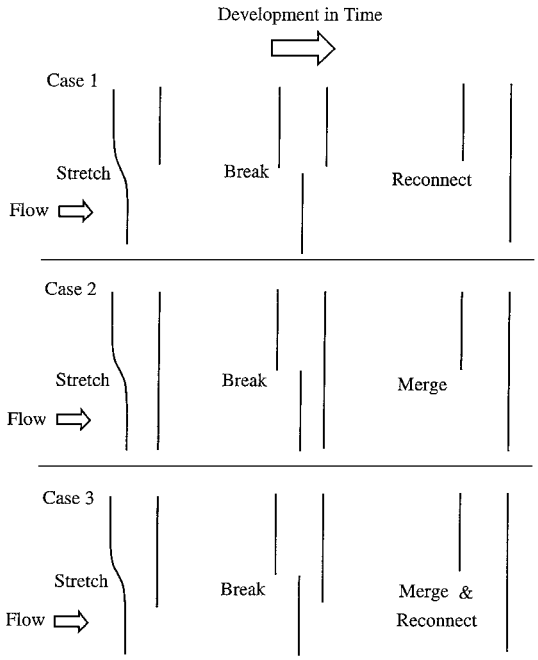

Fig. 6 Three possible processes for the traveling convergent lines.

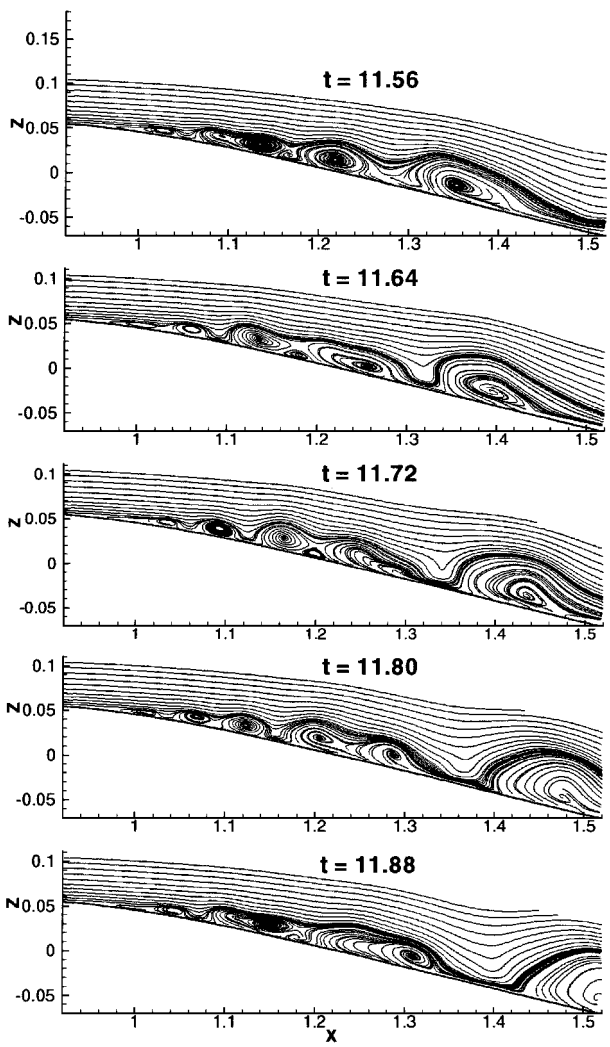

Fig. 7 Limiting streamlines on the x–z plane cutting the hydrofoil at $\eta = 20$ for five different time steps.

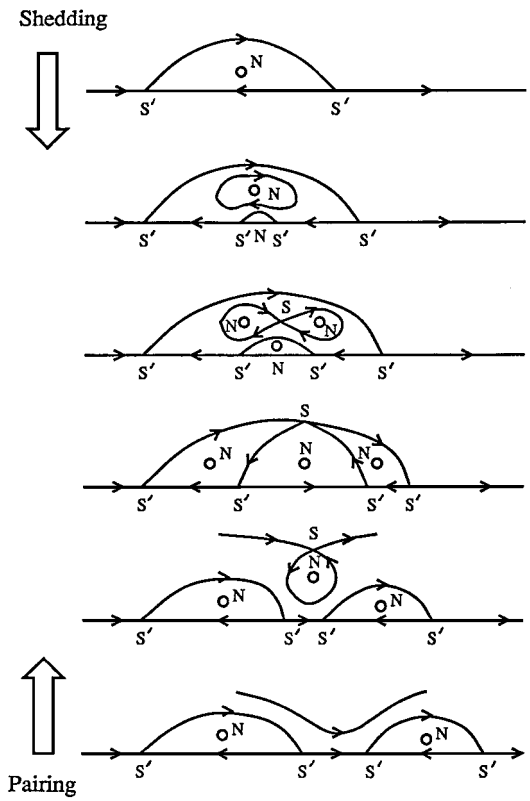

Fig. 8 Sketch of the topological structure of vortex shedding and pairing.

the sketch of the process of vortex shedding and pairing. It is important to note that the topological structure at each step shown in Fig. 8 satisfies the topological rule [Eq. (2)] if one imagines the topological structure occurring on a two-dimensional foil with half-saddles at the leading and trailing edges.

Although vortex shedding and pairing are time processes, their topological development can also occur in space. An example of this is the limiting streamlines on the x–z plane cutting the hydrofoil at five consecutive η locations in the y (spanwise) direction as shown in Fig. 9. The topological structures indicated in Fig. 9 are similar to those of Fig. 8.

The flow structure downstream of the 75% chord is highly three-dimensional and more irregular. Whether the irregular behavior of the flow structure will become regular if the computation is continued is uncertain. In this region the existence of multiple shedding frequencies and three-dimensional pairing processes may lead to a smearing over the entire frequency range because of the interaction between these disturbances, which suggests that a limit-cycle process will never occur.

IV. Unsteadiness of Tip Vortex

From Fig. 4 one can see that the spanwise-shedding vortex is very close to the tip vortex. Therefore, it is expected that the spanwise-shedding vortex will periodically join the tip vortex. To better understand how the spanwise-shedding vortex modifies the tip vortex, streamwise vorticity in a η–ζ plane projected onto the crossflow plane (y–z plane) at six streamwise locations ($\xi = 97, 103, 109, 115, 121, 127$) is compared at two different time steps ($t = 11.56$ and 12.20) and shown in Figs. 10 and 11. Each η–ζ plane location is identified by the streamwise position of the vortex center as indicated in the caption. From Fig. 10 one can see that a strong-shedding vortex sheet continues to roll into the tip-vortex downstream of the trailing edge. One expects that the strength of the tip vortex will be enhanced as the positive vortex sheet rolls up into the tip vortex and is attenuated by the negative vorticity interaction within the tip vortex. The streamwise vorticity along the tip-vortex core, which is evaluated at the location of the minimum-pressure coefficient at each y–z plane, is shown in Fig. 12 for $t = 11.56$. Along the tip-vortex core there are two main peaks of streamwise vorticity

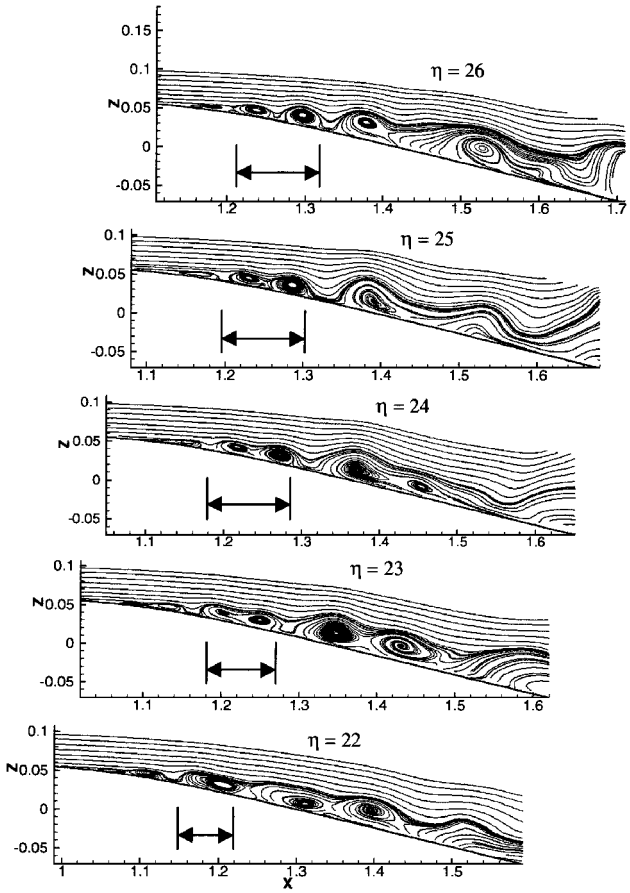

Fig. 9 Limiting streamlines on the x–z plane cutting the hydrofoil at five consecutive η locations in the y (spanwise) direction at $t = 11.56$.

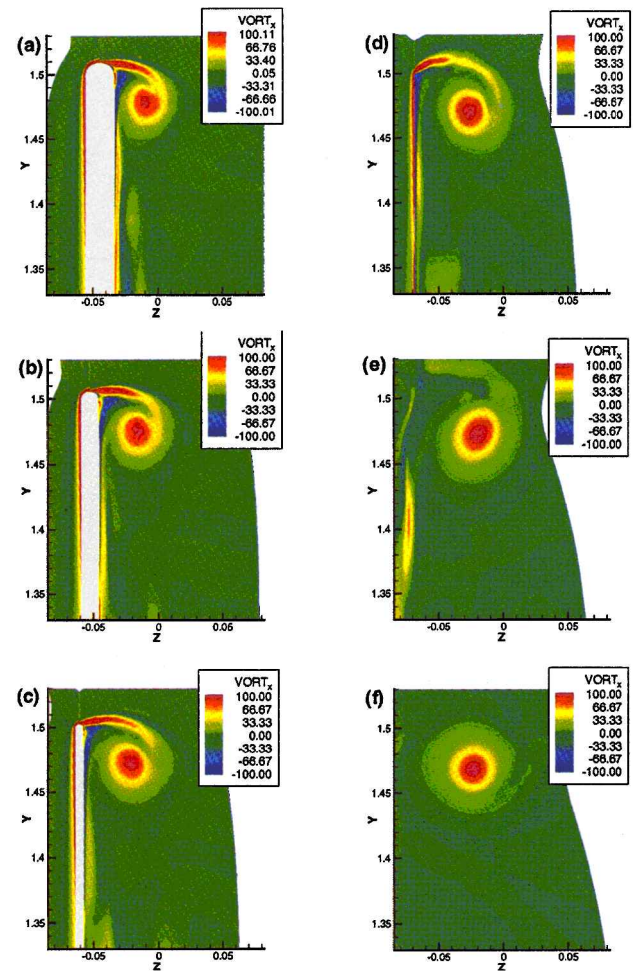

Fig. 10 Projection of the streamwise vorticity on the η–ζ plane for the swept hydrofoil at $t = 11.56$ with the vortex core at a) $x/c = 1.69$, b) $x/c = 1.75$, c) $x/c = 1.81$, d) $x/c = 1.87$, e) $x/c = 1.95$, and f) $x/c = 2.18$.

occurring at $x/c = 1.98$ and 2.12. The first peak is caused by the upper vortex sheet extending from the hydrofoil tip and rolling into the tip vortex. The second peak is produced by the rollup of the lower vortex sheet originating from the suction side of the hydrofoil. The valley between the two peaks is caused by the negative vorticity interacting with the tip vortex. After the tip vortex completely rolls up, the magnitude of streamwise vorticity decreases downstream because of vortex diffusion.

From comparison between Figs. 10 and 11, one can see that an additional clockwise-rotating vortex (rotating in the same direction as the tip vortex) is formed below and to the left of the tip vortex at $t = 12.20$. This clockwise-rotating vortex is the spanwise-shedding vortex, which gradually turns into a streamwise vortex. The roll-up process of the tip-vortex downstream of the trailing edge was altered when the spanwise-shedding vortex joins the tip vortex. Comparison of Figs. 11 and 12 shows that the upper vortex sheet roll up is delayed further downstream at $t = 12.20$ so that the complete roll-up of the upper and lower vortex sheets occurs almost at the same streamwise location. This interaction also results in a different distribution of streamwise vorticity along the tip-vortex core, as shown in Fig. 12.

Because the spanwise-shedding vortex was found to join the tip vortex periodically near the trailing edge, the variation of the streamwise vorticity described in the preceding is expected to occur in a periodic manner. The same behavior is expected to be found in the pressure coefficient along the tip-vortex core because the variation in the streamwise vorticity corresponds to the pressure-coefficient distribution.

V. Effect of Hydrofoil Planform

In the preceding sections only the swept hydrofoil was investigated. A comparison between the swept and unswept hydrofoil for a steady-state flow was made by Hsiao and Pauley.[13] The major difference between the swept and unswept hydrofoil cases was that a secondary flow was induced from the root to the tip on a swept hydrofoil. This secondary flow can carry the low-momentum boundary-layer flow near the tip on the suction side toward the tip vortex. Without this secondary flow the boundary-layer flow was carried toward the root. Therefore, one expects that the laminar-separated flow on the suction side for an unswept hydrofoil will not feed into the tip vortex. The low-frequency tip-vortex fluctuation observed in the swept hydrofoil case may not occur for the unswept hydrofoil.

To demonstrate the effect of hydrofoil planform on the unsteady separated flow, the limiting streamlines on the unswept hydrofoil at $t = 6.9$ are shown in Fig. 13. A significant difference in the topological structure between the swept and unswept hydrofoils occurs near the root section. The outward secondary flow on the swept hydrofoil causes a highly three-dimensional separation near the root section, and the two-dimensional separation is confined to a very small span near the root. For the unswept hydrofoil the separation is nearly two-dimensional across a much larger region near the root section. The spanwise vortex shedding that occurs along the span down to the root section for the unswept hydrofoil gradually extends to the tip as time progresses. The extension of the spanwise vortex shedding, however, stops by the time $t = 7.0$.

Comparison of Figs. 4 and 13 shows that the secondary flow induced by the swept hydrofoil causes the node to form much closer to the hydrofoil tip. The secondary flow is found not only to have a profound effect on the topological structure of the three-dimensional separation but also to influence significantly the interaction between the tip vortex and the spanwise-shedding vortex. Unlike the swept hydrofoil, the spanwise-shedding vortex is carried downward to the root by the secondary flow across the tip for the unswept hydrofoil. The tip vortex is, therefore, quite distinct from the spanwise-shedding vortex in the near-field region. In the two-dimensional study of Lin,[16] the shedding vortex was known to

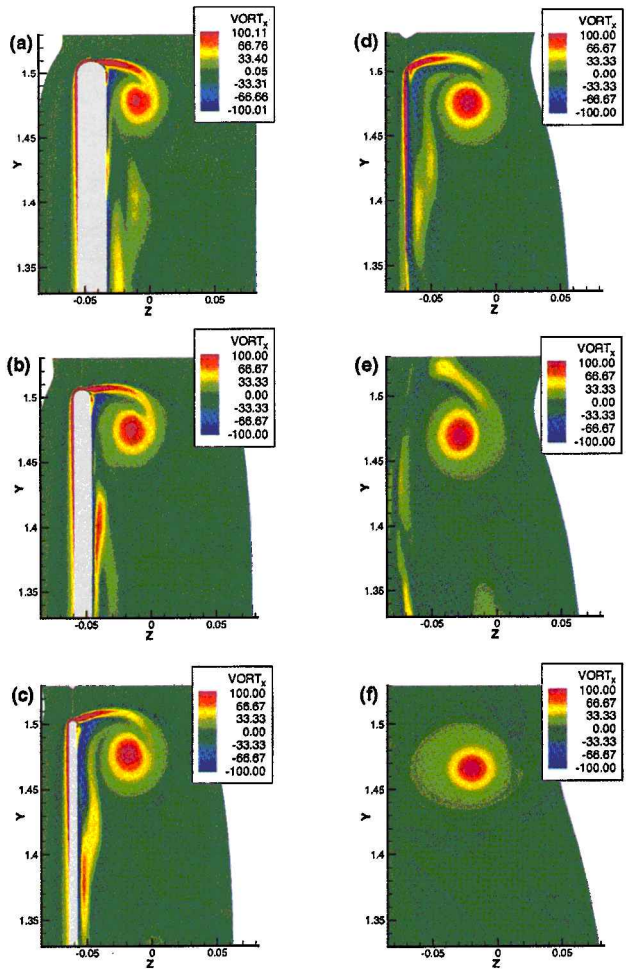

Fig. 11 Projection of the streamwise vorticity on the η–ζ plane for the swept hydrofoil at $t = 12.20$ with the vortex core at a) $x/c = 1.69$, b) $x/c = 1.75$, c) $x/c = 1.81$, d) $x/c = 1.87$, e) $x/c = 1.95$, and f) $x/c = 2.18$.

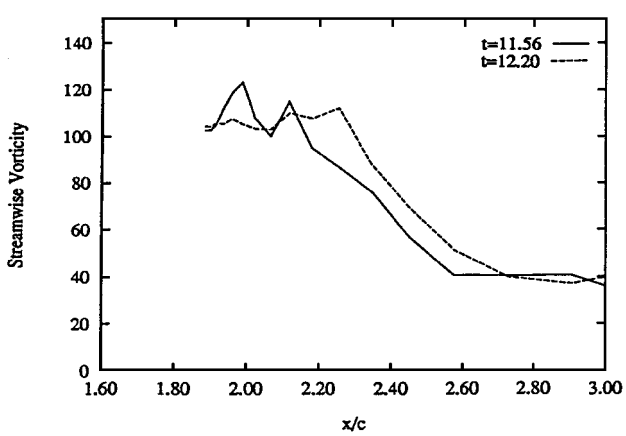

Fig. 12 Distribution of streamwise vorticity along the tip-vortex core for the swept hydrofoil at two time steps.

be dissipated quickly by the wake behind the trailing edge when the shedding vortex passed the trailing edge. Although the shedding vortex sheet behind the hydrofoil will finally roll into the tip vortex in the far-field region, the dissipated vortex cannot significantly influence the tip-vortex core. Therefore the vorticity and pressure distribution along the tip-vortex core in the near-field region, where cavitation inception usually occurs, will not be modified by the spanwise-shedding vortex. The streamwise vorticity contour in a η–ζ plane projected on the crossflow plane (y–z plane) at six streamwise locations for $t = 7.45$ is shown in Fig. 14. The tip vortex in the near-field region was not modified by the spanwise-shedding vortex.

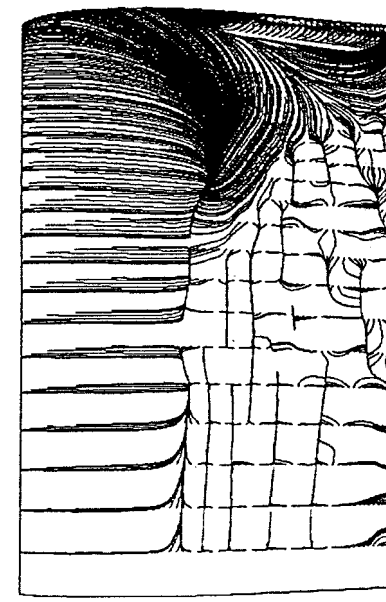

Fig. 13 Limiting streamlines on the unswept hydrofoil at $t = 6.93$.

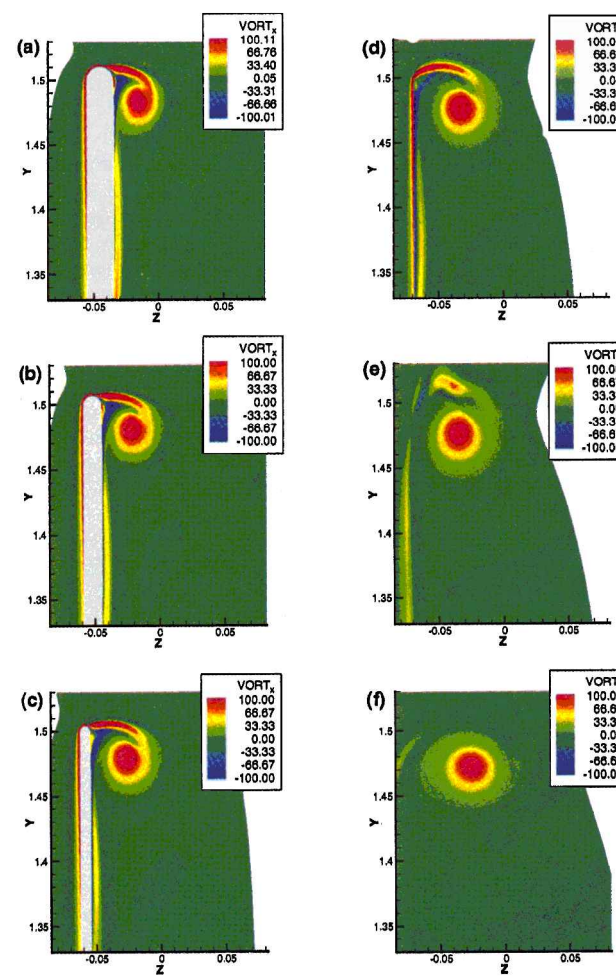

Fig. 14 Projection of the streamwise vorticity on the η–ζ plane for the unswept hydrofoil at $t = 7.45$ with the vortex core at a) $x/c = 0.83$, b) $x/c = 0.89$, c) $x/c = 0.95$, d) $x/c = 1.01$, e) $x/c = 1.09$, and f) $x/c = 1.32$.

The pressure distribution along the tip-vortex core at two time steps for the unswept and swept hydrofoils is shown in Fig. 15. The tip trailing edge is at $x/c = 0.997$ for the unswept and $x/c = 1.863$ for the swept hydrofoil. The pressure distribution of the vortex core from the unswept case remains nearly steady while the pressure distribution from the swept case is significantly unsteady. This comparison also shows that the unswept hydrofoil has larger negative pressure coefficient along the tip-vortex core.

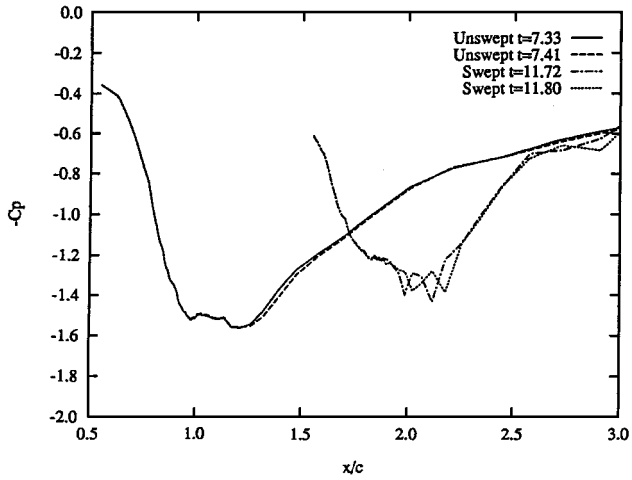

Fig. 15 Distribution of the pressure coefficient along the tip-vortex core for the swept and unswept hydrofoils at two time steps.

Although only two cases, swept and unswept hydrofoils, are compared, some general trends can be assessed. One expects that as the sweep angle is increased the secondary flow induced by the sweep angle will become stronger, and the spanwise-shedding vortex will be carried closer to the tip vortex. As a consequence, one can conclude that the interaction between the spanwise-shedding vortex and the tip vortex will become stronger as the sweep angle is increased.

VI. Conclusions

The development of three-dimensional unsteady separated flow was numerically simulated from an impulsive start. A spanwise vortex was found to shed from the three-dimensional separation bubble after an initial development. The spanwise vortex shedding reached a repeatable limit cycle after a transient development. The topology of the limiting streamlines on the hydrofoil surface at any instantaneous time step was found to satisfy the topological rule.

The spanwise-shedding vortex was found to break into segments then reconnect and/or merge into another shedding vortex because of the streamwise adverse-pressure gradient variation across the span. Three possible processes were identified to describe the phenomena. These three processes produced a spanwise, spatial topological development similar to that of vortex shedding and pairing found temporally.

For the swept hydrofoil a spanwise-shedding vortex near the tip was found to join the tip vortex periodically near the tip trailing edge. This shedding vortex interfered with the tip-vortex roll up in the near-field region. As a consequence, the distribution of the pressure coefficient along the tip-vortex core was altered when the shedding vortex joined the tip vortex.

From the comparison between the swept and unswept hydrofoil, the secondary flow induced by the swept planform was found not only to have a profound effect on the topological structure of the three-dimensional separation, but also to enhance significantly the interaction between the tip vortex and the spanwise-shedding vortex. For the rectangular planform hydrofoil the pressure-coefficient distribution along the tip-vortex core was found to remain nearly steady at the fully developed stage.

Acknowledgments

This research has been supported by the Office of Naval Research under Contract N00014-90-J-1169, monitored by Edwin P. Rood. Computational facilities were provided by the NAVOCEANO Supercomputer Center and the U.S. Army Corps of Engineers Waterways Experiment Station Major Shared Research Center. These contributions are gratefully acknowledged.

References

[1]Green, S. I., and Acosta, A. J., "Unsteady Flow in Trailing Vortices," *Journal of Fluid Mechanics*, Vol. 227, June 1991, pp. 107–134.

[2]Maines, B. H., and Arndt, R. E., "The Case of the Singing Vortex," *Cavitation and Multiphase Flow*, Fluids Engineering Div. Vol. 210, American Society of Mechanical Engineers, New York, 1995, pp. 69–74.

[3]Arndt, R. E. A., Arakeri, V. H., and Higuchi, H., "Some Observations of Tip-Vortex Cavitation," *Journal of Fluid Mechanics*, Vol. 229, Aug. 1991, pp. 269–289.

[4]Lin, J. C. M., and Pauley, L. L., "Low-Reynolds-Number Separation on an Airfoil," *AIAA Journal*, Vol. 34, No. 8, 1996, pp. 1570–1577.

[5]Wilson, P. G., and Pauley, L. L., "Two- and Three-Dimensional Large-Eddy Simulations of a Transitional Separation Bubble," *Physics of Fluids*, Vol. 10, No. 11, 1998, pp. 2932–2940.

[6]Tobak, M., and Peake, D. J., "Topology of Three-Dimensional Flow Separations," *Annual Review of Fluid Mechanics*, Vol. 14, 1982, pp. 61–85.

[7]Hornung, H. G., and Perry, A. E., "Some Aspects of Three-Dimensional Separation, Part I: Streamsurface Bifurcations," *Zeitschrift für Flugwissenschaften und Weltraumforschung*, Vol. 8, No. 2, 1984, pp. 77–87.

[8]Hui, W. H., and Tobak, M., "Topology of Steady and Unsteady Incompressible Three-Dimensional Separated Flows," *Continuum Mechanics and Its Applications*, edited by G. A. Graham and S. K. Malik, Hemisphere, New York, 1989, pp. 519–541.

[9]Dallmann, U., and Schewe, G., "On Topological Changes of Separating Flow Structures at Transition Reynolds Number," AIAA Paper 87-1266, June 1987.

[10]Pauley, L. L., "Structure of Local Pressure-Driven Three-Dimensional Transient Boundary-Layer Separation," *AIAA Journal*, Vol. 31, No. 5, 1994, pp. 997–1005.

[11]Rogers, S. E., Kwak, D., and Kiris, C., "Steady and Unsteady Solutions of the Incompressible Navier–Stokes Equations," *AIAA Journal*, Vol. 29, No. 4, 1991, pp. 603–610.

[12]Roe, P. L., "Approximate Riemann Solvers, Parameter Vectors, and Difference Schemes," *Journal of Computational Physics*, Vol. 43, No. 2, 1981, pp. 357–372.

[13]Hsiao, C.-T., and Pauley, L. L., "Numerical Study of the Steady-State Tip Vortex Flow over a Finite-Span Hydrofoil," *Journal of Fluids Engineering*, Vol. 120, No. 2, 1998, pp. 345–353.

[14]Mehta, U., "Verification and Validation of Computer Simulations," Keynote Address, American Society of Mechanical Engineers, Fluids Engineering Div. Summer Meeting, San Diego, CA, July 1996.

[15]Dacles-Mariani, J., Rogers, S., Kwak, D., Zilliac, G., and Chow, J. S., "Numerical/Experimental Study of a Wingtip Vortex in the Near Field," *AIAA Journal*, Vol. 33, No. 9, 1995, pp. 1561–1568.

[16]Lin, J. C. M., "Numerical Investigation of the Unsteady Large-Scale Structure in Laminar Separation Bubbles," Ph.D. Dissertation, Dept. of Mechanical Engineering, Pennsylvania State Univ., University Park, PA, Sept. 1993.

[17]Perry, A. E., and Chong, M. S., "A Description of Eddying Motions and Flow Patterns Using Critical-Point Concepts," *Annual Review of Fluid Mechanics*, Vol. 19, 1987, pp. 125–155.

[18]Henk, R. W., Reynolds, W. C., and Reed, H. L., "An Experimental Investigation of the Fluid Mechanics of an Unsteady, Three-Dimensional Separation," Dept. of Mechanical Engineering, Stanford Univ., Rept. TF-49, Stanford, CA, Aug. 1990.

[19]Pauley, L. L., Moin, P., and Reynolds, W. C., "The Structure of Two-Dimensional Separation," *Journal of Fluid Mechanics*, Vol. 220, Nov. 1990, pp. 397–441.

P. R. Bandyopadhyay
Associate Editor